ENVIRONMENTAL RESEARCH
LETTERS

LETTER

Multidecadal variation of northern hemisphere summer monsoon forced by the SST inter-hemispheric dipole

Jiaqing Xue[1], **Bingchao Wang**[1,2], **Yongkui Yu**[1], **Jianping Li**[3,6,*], **Cheng Sun**[4] **and Jiangyu Mao**[5]

[1] Key Laboratory of Meteorological Disaster of Ministry of Education/Joint International Research Laboratory of Climate and Environment Change/Collaborative Innovation Center on Forecast and Evaluation of Meteorological Disasters/Institute for Climate and Application Research, Nanjing University of Information Science and Technology, Nanjing, People's Republic of China
[2] Guiyang Meteorological Bureau, Chenzhou, People's Republic of China
[3] Frontiers Science Center for Deep Ocean Multispheres and Earth System/Key Laboratory of Physical Oceanography/Institute for Advanced Ocean Studies, Ocean University of China, Qingdao, People's Republic of China
[4] College of Global Change and Earth System Science, Beijing Normal University, Beijing, People's Republic of China
[5] State Key Laboratory of Numerical Modeling for Atmospheric Sciences and Geophysical Fluid Dynamics, Institute of Atmospheric Physics, Chinese Academy of Sciences, Beijing, People's Republic of China
[6] Laboratory for Ocean Dynamics and Climate, Pilot Qingdao National Laboratory for Marine Science and Technology, Qingdao, People's Republic of China
[*] Author to whom any correspondence should be addressed.

E-mail: ljp@ouc.edu.cn

Keywords: SST inter-hemispheric dipole, northern hemisphere summer monsoon, decadal variability

Supplementary material for this article is available online

OPEN ACCESS

RECEIVED
4 September 2021

REVISED
18 January 2022

ACCEPTED FOR PUBLICATION
3 March 2022

PUBLISHED
21 March 2022

Abstract

The sea surface temperature inter-hemispheric dipole (SSTID) is an important variability mode of global SST anomalies, characterized by an anti-phase variation of SST between the two hemispheres. In this study, the decadal variation of the northern hemisphere summer monsoon (NHSM) is found to be strongly regulated by the SSTID, with positive (negative) phases of the SSTID corresponding to the strengthening (weakening) of NHSM. Both observation and SST-forced atmospheric model simulations suggest that the SSTID related thermal forcing modulates the NHSM by causing planetary-scale atmospheric circulation adjustments. Positive SSTID events lead to coherent increase (decrease) of surface air temperature over the entire northern (southern) hemisphere, increasing the inter-hemispheric thermal contrast (ITC). As sea level pressure changes are just opposite to air temperature, the increase of ITC enhances the inter-hemispheric pressure gradient (southern hemisphere minus northern hemisphere), leading to the strengthening of summer monsoonal circulation and the increase of monsoon rainfall in the northern hemisphere.

1. Introduction

The monsoon, a spectacular phenomenon in Earth's climate system, manifests as a forced response of the coupled ocean–atmosphere–land system to the annual cycle of solar radiation (Trenberth *et al* 2000). Besides the seasonal reversal of surface winds, monsoon is also accompanied by prominent changes in precipitation. About two-thirds of the world's population lives in monsoon regions, and the evolution and variation of the monsoon system thus have profound impacts on human society (Wang and Ding 2006, Zhang *et al* 2018). Therefore, a better understanding of monsoon variability, especially its changes over land, has the potential to benefit the livelihood of those living in monsoon regions.

Affected by land–sea distribution, the northern hemisphere bears most of the human activities, and this study will hence focus on investigating the variability of the northern hemisphere summer monsoon (NHSM). The sub-systems of NHSM include the West African monsoon, South Asian monsoon, East Asian monsoon, and the North American monsoon (Li and Zeng 2002, Wang *et al* 2013, An *et al* 2015). The decadal variations and driving mechanisms of these regional monsoons have been extensively explored in previous studies (Kripalani *et al* 2003, Lu *et al* 2006, Kucharski *et al* 2009, Li *et al* 2010a,

Yun *et al* 2010, Lopez *et al* 2016). For example, the long-term precipitation record indicates the Indian summer monsoon shows strong decadal variation during the period of 1871–2001, and local Indian Ocean SST forcing is found to has significant contribution to the decadal variation (Kripalani *et al* 2003, Kucharski *et al* 2006). For the African summer monsoon, Hoerling *et al* (2006) investigated the trend of monsoon rainfall since 1950 and found the Sahel drying is an atmospheric response to warming of the South Atlantic relative to North Atlantic sea surface temperature (SST). Moreover, the weakening of East Asian summer monsoon (EASM) since the late 1970s is shown to be associated with the decadal SST warming over the central and eastern Pacific (Zhou *et al* 2009, Li *et al* 2010a). Most of these studies are based on regional perspectives, emphasizing the impacts of local land–sea thermal contrast and topography on monsoon variability. However, on decadal and longer time scales, the monsoon variability is primarily regulated by planetary-scale controls, and the regional perspective is unable to reveal the causes of monsoon decadal variation (Wang *et al* 2013). In view of coherent variations among regional monsoons, it is needed to investigate monsoon decadal variability from a global perspective. Indeed, several earlier studies have examined the recent changes of the global monsoon system (Zhou *et al* 2008, Hsu *et al* 2011, Wang *et al* 2013). For instance, Wang *et al* (2013) found that both circulation and precipitation of the NHSM have shown a significant enhancement since the late 1970s, which is primarily caused by a combined forcing of the Interdecadal Pacific Oscillation (IPO) and Atlantic Multidecadal Oscillation (AMO). However, the research period for these studies is relatively short, mainly focusing on the trend of NHSM, and not able to capture its decadal oscillation. As such, further investigations into the decadal variation of NHSM and its driving mechanism are necessary.

The SST inter-hemispheric dipole (SSTID) is one of the dominant variability modes of global SST anomalies, which is characterized by a decadal-scale seesaw of SST between the northern and southern hemispheres (Folland *et al* 1999, Parker *et al* 2007, Sun *et al* 2013, Chen *et al* 2017). The SSTID is partially related to the AMO in the North Atlantic region, however it differs from AMO in spatial pattern as demonstrated by Sun *et al* (2013). Even though the formation mechanism of the SSTID is still not well understood, both ocean meridional overturning circulation and hemispheric asymmetries in aerosol emissions are found to play important roles in the asymmetric evolution of SST between the two hemispheres (Dima and Lohmann 2010, Chiang and Friedman 2012, Chung and Soden 2017). In previous studies, the SSTID is documented to have significant impacts on the decadal variations of tropical rainfall and extratropical atmospheric circulation over the two hemispheres (Sun *et al* 2013, Lopez *et al* 2016, Xue *et al* 2018a). As a global-scale variability mode on decadal timescales, the SSTID is strongly associated with the changes of an inter-hemispheric thermal gradient, which indicates the SSTID may also exert impacts on the decadal variability of the global monsoon system. Therefore, this study aims to examine the possible influence of SSTID on the decadal variation of NHSM. The remainder of this paper is organized as follows. Datasets and methods are introduced in section 2. Section 3 investigates the impacts of SSTID on NHSM through both observational analysis and SST-forced atmospheric general circulation model (AGCM) simulations. Finally, section 4 contains a summary and discussion.

2. Data and methodology

The gridded SST data is taken from the Extended Reconstructed Sea Surface Temperature version 4, which covers the period from 1854 to the present with a 2° × 2° resolution (Huang *et al* 2015). The monthly land precipitation is based on the Climatic Research Unit Time-Series version 3.23, which is available on a 0.5° × 0.5° grid spanning the period 1901–2014 (Harris *et al* 2014). Atmospheric reanalysis data including surface air temperature, sea level pressure (SLP) and horizontal winds is obtained from the National Centers for Environmental Prediction and National Center for Atmospheric Research, covering the period from 1948 to the present (Kalnay *et al* 1996). Summer in this study refers to the boreal season from May to September (MJJAS).

The regional monsoon is measured by the dynamic normalized seasonality (DNS) index, which delineates the monsoon intensity with the amplitude of seasonal variation of wind field (Li and Zeng 2002). For a given spatial grid point, the DNS index in the mth month of the nth year is expressed as:

$$\delta_{m,n} = \frac{\left\| \vec{V}_1 - \vec{V}_{m,n} \right\|}{\left\| \vec{V} \right\|} - 2, \qquad (1)$$

where $\vec{V}_1$ is the climatological wind vector in January, $\vec{V}$ indicates the average of climatological wind vectors in January and July, and $\vec{V}_{m,n}$ represents the wind vectors in mth month of the nth year. Then the monsoon index is obtained by averaging the 850 hPa DNS index over each monsoon region. The West African summer monsoon index is defined as the area-averaged summer DNS index over 5° N–17.5° N, 20° W–40° E. Similarly, the South Asian summer monsoon (SASM) index is defined as the average over 10° N–25° N, 50° E–100° E, the EASM index is the average over 10° N–45° N, 105° E–130° E, and the North American summer monsoon is the average over 0° N–15° N, 70° W–55° W. The IPO index is calculated as the difference between SST anomalies averaged over the central equatorial Pacific (10° S–10° N,

170° E–90° W) and the average of SST anomalies in the northwest (25° N–45° N, 140° E–145° W) and southwest Pacific (50° S–15° S, 150° E–160° W) following Henley *et al* (2015). The AMO index is defined as the area-weighted average of SST anomalies over the North Atlantic region (0° N–65° N) (Enfield *et al* 2001).

The Student's *t*-test is employed to determine the statistical significance of correlation and regression coefficients. Considering the impact of autocorrelations on degrees of freedom, we use an effective number of degrees of freedom N^{eff} based on the following approximation:

$$\frac{1}{N^{\text{eff}}} \approx \frac{1}{N} + \frac{2}{N}\sum_{j=1}^{N}\frac{N-j}{N}\rho_{XX}(j)\rho_{YY}(j), \qquad (2)$$

where N is the sample size, $\rho_{XX}(j)$ and $\rho_{YY}(j)$ denote the autocorrelations of time series X and Y at time lag j, respectively (Sun *et al* 2017, Xue *et al* 2018b, 2018c).

The SST sensitivity experiments are performed using the International Centre for Theoretical Physics AGCM (ICTPAGCM), which adopts T30 horizontal spectral truncation and includes eight vertical levels (Molteni 2003). This intermediate model has been widely used in the research of monsoon variability (Kucharski *et al* 2006, 2009, Dogar *et al* 2017). In the control run, the model is forced with the climatological mean SST. Along with the control run, three sets of sensitivity experiments are conducted with forcing of summer SSTID anomalies, AMO anomalies and SSTID anomalies removing the AMO signal, respectively. All simulations are integrated for 50 years and the outputs for years 31–50 are analyzed. Moreover, a set of Atmospheric Model Intercomparison Project (AMIP) experiment based on NASA GISS Model E2-R in phase 5 of the Coupled Model Intercomparison Project is also used (Taylor *et al* 2012). This model is chosen because of its availability of long-term simulations, which make it possible to obtain reliable atmospheric responses to SST forcing. The AMIP experiment is run from 1880 to 2010 with prescribed historical SST and includes five ensemble members (r1i1p1–r5i1p1). The years 1880–1899 of all simulations are regarded as spin-up, and the analysis is performed on the remaining period of 1900–2010. To highlight the SST-forced atmospheric responses, we analyze the results based on the average of five ensemble members.

3. Results

3.1. Spatio-temporal characteristics of the SSTID in summer

Figure 1(a) gives the normalized time series of summer SSTID index, which is defined as the difference of hemispheric-mean SST anomalies between the northern and southern hemispheres following past studies (Sun *et al* 2013, Xue *et al* 2018a). The SSTID index is observed to exhibit strong decadal variability, including three main decadal phase shifts during the 20th century. The summer SSTID pattern is then obtained as the correlation map between SSTID index and global SST anomalies. As seen in figures 1(b) and (c), the SSTID is characterized by an inter-hemispheric dipolar pattern with opposite-signed SST anomalies between the two hemispheres.

It is noted that the SSTID related SST anomalies in the North Atlantic is similar to the AMO pattern (Enfield *et al* 2001, Lyu *et al* 2017). As a regional mode in the North Atlantic, AMO is asymmetric about the equator and thus contribute to the formation of SSTID. Therefore, SSTID is not completely independent of the AMO, and there exists connection between them. However, there are prominent differences between these two phenomena. Figure S1 (available online at stacks.iop.org/ERL/17/044033/mmedia) further shows the partial correlation between SSTID index and global SST anomalies with the AMO influence being linearly removed. After removing AMO, the SSTID signal is found to be weakened in the North Atlantic, but basically unchanged in other ocean basins. Moreover, the decadal variability of SSTID index still exists even removing the AMO signal (figure S2). As such, the spatio-temporal evolution of the SSTID is demonstrated to be largely independent of the AMO, and the AMO can be regarded as the North Atlantic component of the SSTID. In addition, as an equatorial asymmetric mode, the SSTID is independent of the IPO that is symmetric about the equator, and the SSTID pattern is thus found to be unchanged when the IPO signal is removed (figure S1(b)).

The inter-hemispheric dipolar pattern of SSTID indicates its potential influence on trans-hemispheric SST gradient over the tropics. To confirm this, figure 1(d) calculates the correlation between SSTID index and zonal-mean meridional SST gradients in summer. The meridional SST gradients over the tropics are found to be significantly increased during positive phases of the SSTID. In this regard, the SSTID may influence the decadal variation of summer monsoon system by modulating the inter-hemispheric thermal contrast (ITC).

3.2. The relationship between the SSTID and decadal variation of NHSM

Figure 2(a) presents the differences in land precipitation and 850 hPa winds between summer and winter based on the 1961–1990 climatology. Areas with notable precipitation changes in the northern hemisphere are located mainly in the tropical regions of West Africa, South Asia, East Asia, and North America. Since precipitation are closely related to the

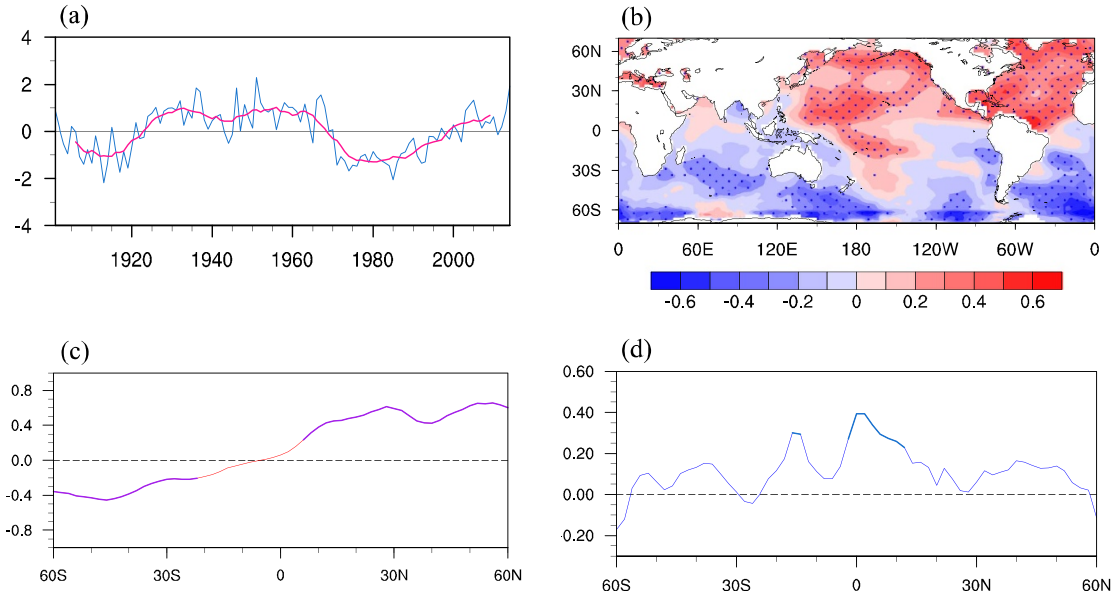

Figure 1. (a) Normalized time series of summer SSTID index during 1901–2014 and its 11-year running mean. (b) Correlation map between the SSTID index and global SST anomalies in summer. (c) Correlation between the SSTID index and zonal mean SST anomalies in summer. (d) As in (c), but for meridional SST gradients and SSTID index. Dotted shading and bolded lines indicate correlations above the 95% confidence level.

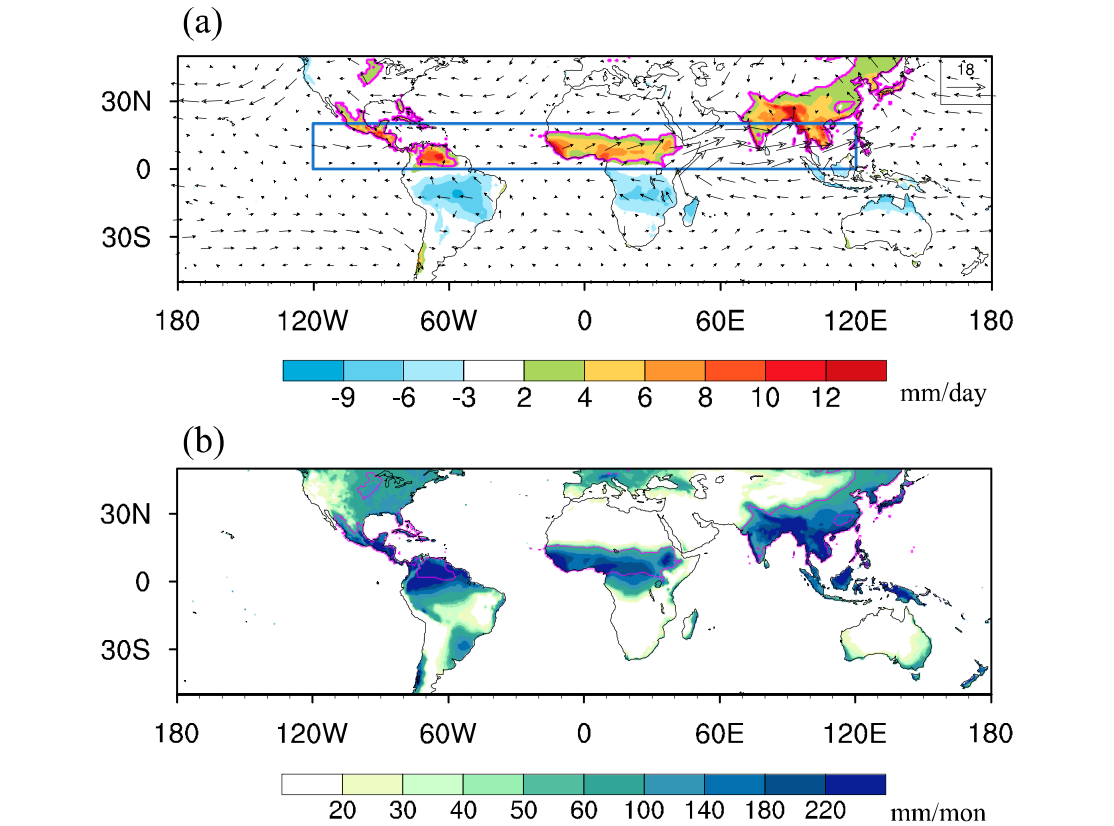

Figure 2. (a) Climatological mean MJJAS minus NDJFM rainfall (shading; mm d^{-1}) and 850 hPa winds (vectors; m s^{-1}). The land monsoon area in the northern hemisphere is outlined by pink lines. The boxed area indicates a key domain (0° N–20° N, 120° W–120° E) for monsoon circulation. (b) The collocation between climatological summer precipitation (shading; mm $month^{-1}$) and northern hemisphere land monsoon area indicated by pink lines.

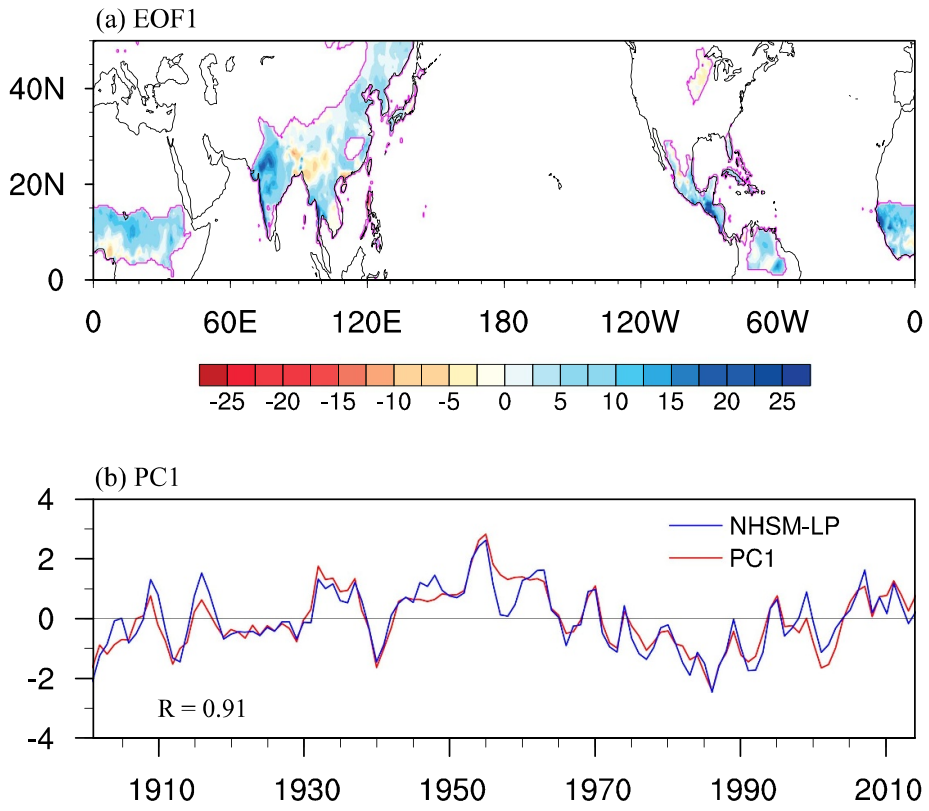

Figure 3. The (a) spatial pattern and (b) principal component of the first EOF mode of 3 years running averaged summer precipitation over northern hemisphere land monsoon region during 1901–2014. The time series of the NHSM-LP index is also shown as a blue line in (b).

atmospheric circulation, seasonal variations of precipitation are meanwhile accompanied by the seasonal reversal of low-level winds. And regions with the most prominent wind changes are over a zonal band extending from the Mexico to Philippines (0° N–20° N, 120° W–120° E). Based on the seasonal variation of land precipitation, the monsoon regions are identified as areas where the difference of precipitation rates between summer and winter exceeds 2 mm d^{-1}, and summer precipitation exceeds 55% of the total annual precipitation (Wang *et al* 2013). The blue lines in figure 2(a) outline the distribution of northern hemisphere land monsoon area. Moreover, figure 2(b) shows the collocation between northern hemisphere land monsoon region and summer precipitation. It is found that summer precipitation mainly occurs over the monsoon region, indicating monsoon rainfall is the main source of summer precipitation for the northern hemisphere. Therefore, understanding the variability and driving mechanism of NHSM is of great importance.

To reveal the dominant variability mode of NHSM, figure 3(a) presents the first empirical orthogonal function mode (EOF1) of summer precipitation over the northern hemisphere land monsoon area. The spatial pattern of EOF1 is characterized by coherent changes over the entire monsoon region. According to this feature, the intensity of NHSM can be measured simply by the area-averaged precipitation rate over the land monsoon region, referred to as the NHSM land precipitation (NHSM-LP) index. The NHSM-LP index is highly consistent with the principle component of EOF1 with a positive correlation of 0.91, which is significant at the 95% confidence level (figure 3(b)). The NHSM-LP index displays prominent decadal oscillation, with three main phase changes during the 20th century (figure 4(a)). To understand the causes of NHSM decadal variation, figure 4(b) examines the decadal-scale correlation between NHSM-LP index and global SST anomalies. The most prominent feature of the correlation map is opposite-signed values between the two hemispheres, basically with positive correlations in the northern hemisphere and negative correlations in the southern hemisphere. Moreover, the pattern is found to project onto the IPO signal over the Pacific sector, and this is because the IPO has certain modulating effects on the decadal variation of NHSM, as documented in Wang *et al* (2013). In order to explore the possible influence of SST variability other than IPO on the NHSM, figure 4(c) further calculates the partial correlation between NHSM-LP

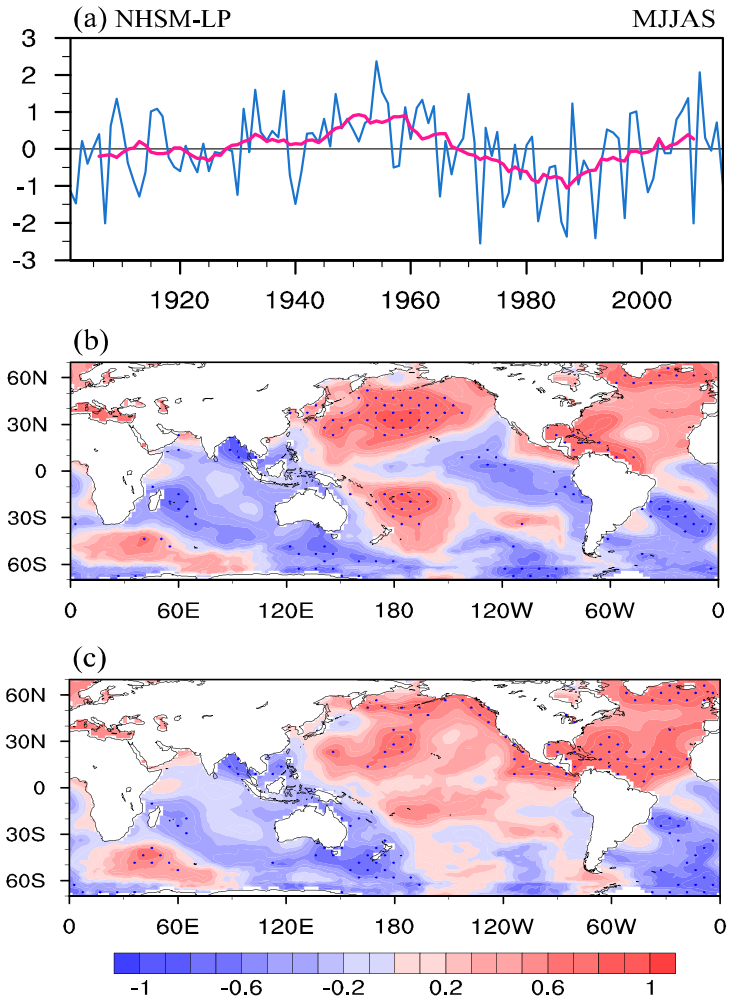

Figure 4. (a) Normalized time series of NHSM-LP index (blue) and its 11-year running mean (pink) during 1901–2014. (b) Decadal-scale correlation between NHSM-LP index and global SST anomalies in summer during 1901–2014. (c) As in (b), but for the partial correlation with IPO influence being removed. Dotted shading indicates correlations significant at the 90% confidence level.

index and SST anomalies with the IPO influence being linearly removed. After excluding the IPO influence, we can see the correlation map shows a prominent inter-hemispheric dipolar pattern, reminiscent of the SSTID. Figure 5 thus compares the normalized time series of the NHSM-LP and summer SSTID indices. The decadal variation of NHSM is found to be strongly in phase with the SSTID with a positive correlation of 0.82, exceeding the 95% confidence level (figure 5(a)). Furthermore, the consistency of phase evolution between the NHSM and SSTID is enhanced when the IPO influence is removed (figure 5(b)). Based on the results of multiple linear regression reconstruction, we found the combined influence of the IPO and SSTID well explains the decadal variation of NHSM. Meanwhile, the reconstructed results are basically unchanged when the AMO signal is removed from the SSTID (figure S3).

The above statistical results indicate that the SSTID may have an important modulating effect on the decadal variation of NHSM. To illuminate physical mechanisms responsible for the influence of the SSTID on NHSM, we investigate the anomalous changes in low-level atmospheric variables, including surface air temperature, SLP and 850 hPa winds. During the positive phases of the SSTID, surface air temperature increase coherently over the entire northern hemisphere while the air temperature in the southern hemisphere decreases, this is consistent with the spatial pattern of the SSTID (figure 6(a)). Accompanying the northern hemisphere warming, the SLP shows a hemispheric-scale lowering, with centers of negative anomalies located in a zonal band extending from the tropical Atlantic to the Eurasian continent north of the Tibet Plateau. The low-pressure anomalies lead to strengthened monsoon circulation in the northern hemisphere and enhanced water vapor convergence into the monsoon region, thus increasing the NHSM rainfall (figures 6(b) and (c)).

The above analysis indicates the SSTID is accompanied by a hemispheric adjustment of atmospheric

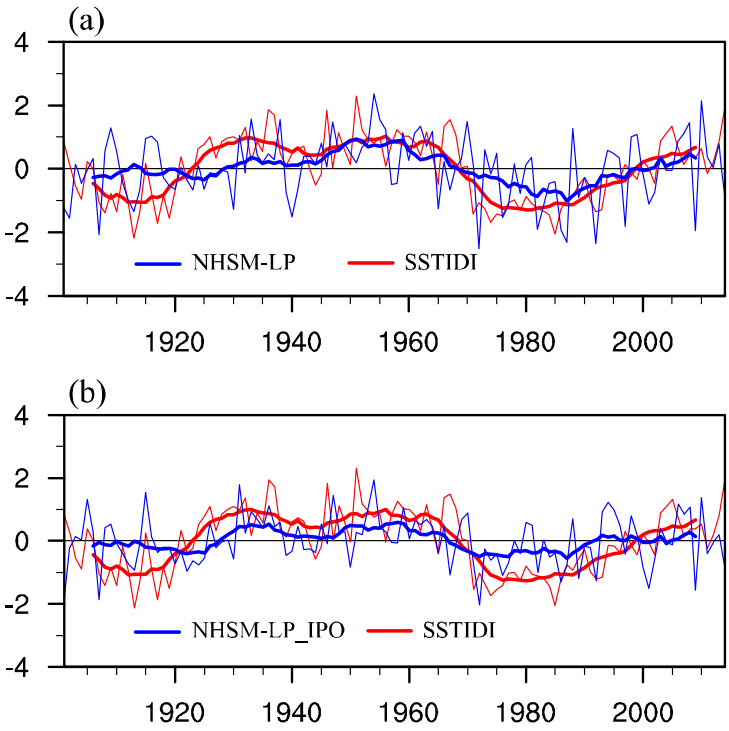

Figure 5. (a) Normalized time series of NHSM-LP and SSTID indices in boreal summer and their 11-year running means. (b) As in (a), but with the IPO influence being removed from the NHSM-LP index.

circulation. On this basis, figure 7 further analyzes the time evolution between the SSTID and planetary-scale atmospheric circulation. First, the ITC is defined as the difference of averaged surface air temperature between the northern and southern hemispheres. The decadal variation of ITC is found to be positively correlated with the SSTID, with a correlation coefficient of 0.8 (figure 7(a)). As for SLP, the inter-hemispheric pressure contrast (IPC) and SSTID shows a prominent inverse variation on decadal timescales and the correlation between the two reaches −0.94 (figure 7(b)). The positive SSTID corresponds to temperature increase (decrease) in the northern (southern) hemisphere, increasing the temperature difference between the two hemispheres. And such an increase in ITC intensifies the south–north pressure gradient (southern hemisphere minus northern hemisphere), enhancing the northward trans-equatorial airflow for the monsoon region (figure 7(c)). As northern hemisphere monsoon is characterized by notable seasonal variation of wind field over 0° N–20° N; 120° W–120° E (figure 2(a)), the average zonal wind in this domain can be used to characterize the variation of planetary-scale monsoon circulation. As demonstrated in figure 7(d), there is a good synchronous evolution between the SSTID and zonal wind index (the correlation coefficient reaches 0.94), which indicates the NHSM circulations are strengthened during the positive phases of the SSTID.

The NHSM comprises several monsoon subsystems, including the West African monsoon, South Asian monsoon, East Asian monsoon, and the North American monsoon. Figure 8 further checks the relationship between the SSTID and these regional monsoon systems, respectively. As seen in the figure, each subsystem of NHSM has undergone significant decadal variation during 1948–2014, showing a synchronous weakening from 1960 to 1985 and strengthening from 1990 to the present. It is noted that the decadal variations of these monsoon systems are all consistent with the phase evolution of SSTID, which further demonstrates the SSTID has a modulating effect on the whole NHSM.

3.3. NHSM responses to SSTID forcing in AGCM simulations

The decadal variations of NHSM rainfall and circulation are observed to be synchronized with the SSTID. And the above analyses suggest that the SSTID may influence NHSM by causing hemispheric-scale atmospheric circulation adjustment through its thermal forcing. To confirm this, both SST-forced sensitivity experiments and AMIP simulations are employed to verify the NHSM responses to SSTID forcing. First, three sets of sensitivity experiments are conducted with forcing of summer SSTID anomalies, AMO anomalies and residual SSTID anomalies with the AMO signal being removed, respectively (figure S4). Figure 9 shows the NHSM rainfall responses to anomalous SST forcing in three sets of AGCM simulations. It is observed from figure 9(a) that the anomalous SSTID forcing can significantly increase the

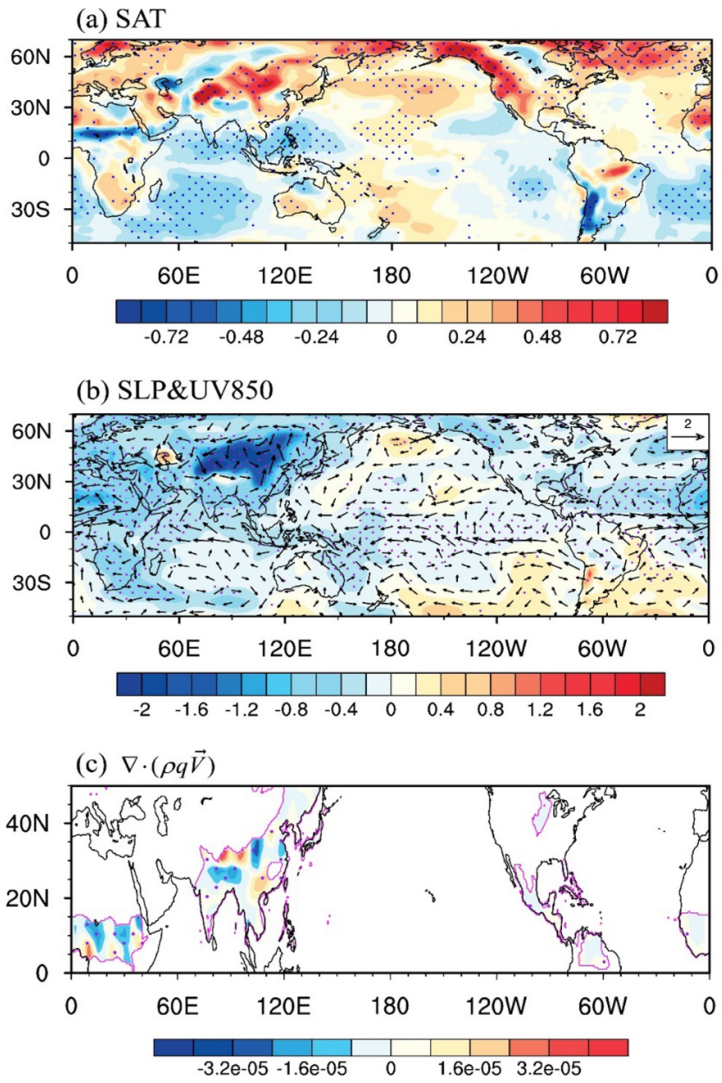

Figure 6. (a) Regression map of anomalous surface air temperature (units: °C) against the normalized SSTID index in summer during the period 1948–2014 on decadal time scales. (b) The same as in (a), but for SLP (shading; units: hPa) and 850 hPa winds (vector; units: m s^{-1}). (c) As in (a), but for the moisture flux divergence (units: g m^{-3} s^{-1}). Dotted shading denotes regressions exceeding the 90% confidence level.

NHSM rainfall, while the impacts of AMO forcing on NHSM is not that significant (figure 9(b)). This demonstrate that the decadal variation of NHSM is better explained by the SSTID than the AMO, which only explains the North Atlantic component of the SSTID. By comparing three sets of AGCM experiments, it is also noted that the influence of SSTID on EASM and SASM is caused by the combined forcing of AMO and residual SSTID anomalies, while the West African summer monsoon is more related to the residual SSTID forcing. As such, the above results indicate that the North Atlantic and Indo-Pacific components of the SSTID combine to modulate the NHSM.

On this basis, the impacts of SSTID is further examined in an AMIP experiment, which is based on more a comprehensive AGCM and has longer integration time. Figure 10 presents the simulated monsoon rainfall response to SSTID forcing. It is demonstrated the positive SSTID can indeed increase monsoon precipitation in the northern hemisphere (figure 10(a)), and the time series of NHSM-LP index is also in phase with the SSTID (figure 10(b)). In addition, figure S5 presents the responses of surface air temperature, SLP and 850 hPa winds to SSTID thermal forcing in the AMIP experiment. As observed in figure S5(a), the SSTID forcing causes divergent responses of surface air temperature between the two hemispheres, with coherent warming (cooling) over the northern (southern) hemisphere. It is, therefore, noted that the SSTID forcing reduces SLP in the northern hemisphere and enhances the south–north pressure gradient (southern hemisphere minus northern hemisphere), hence strengthening the northward trans-equatorial airflow and monsoonal circulation (figure S5(b)). The time

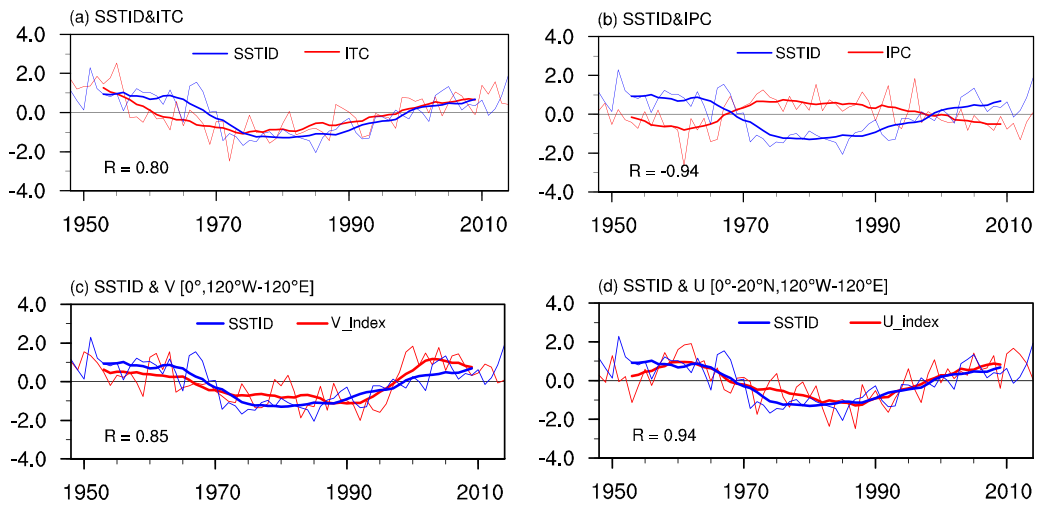

Figure 7. (a) Normalized time series of SSTID (blue) and inter-hemispheric thermal contrast (ITC; defined as the surface air temperature averaged over 20° N–70° N, 120° W–120° E minus that over 40° S–0° S, 120° W–120° E) during 1948–2014 and their 11-year running means. (b)–(d) As in (a), but for SSTID and (b) IPC, (c) 850 hPa cross-equatorial meridional wind averaged over 120° W–120° E and (d) 850 hPa zonal winds averaged over 0° N–20° N, 120° W–120° E. The decadal-scale correlation coefficient (*R*) between the two indices is indicated in each figure.

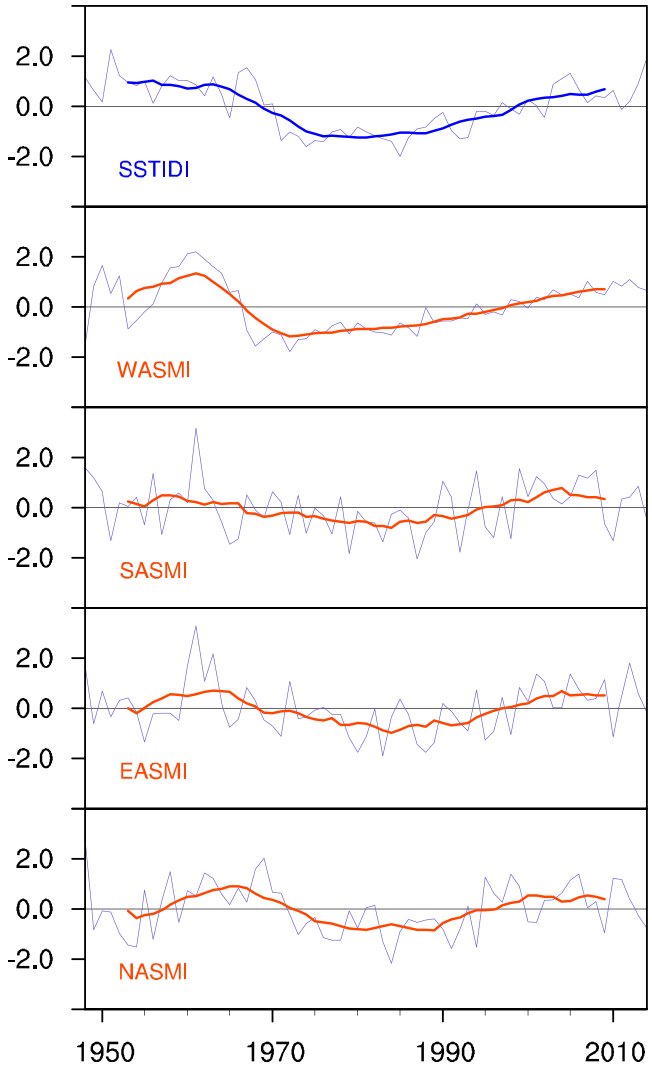

Figure 8. Normalized time series of (a) SSTID index and the (b) West African, (c) South Asian, (d) East Asian, (e) North American summer monsoon indices during 1948–2014 and their 11-year running means. The linear trends during 1948–2014 are removed for all indices.

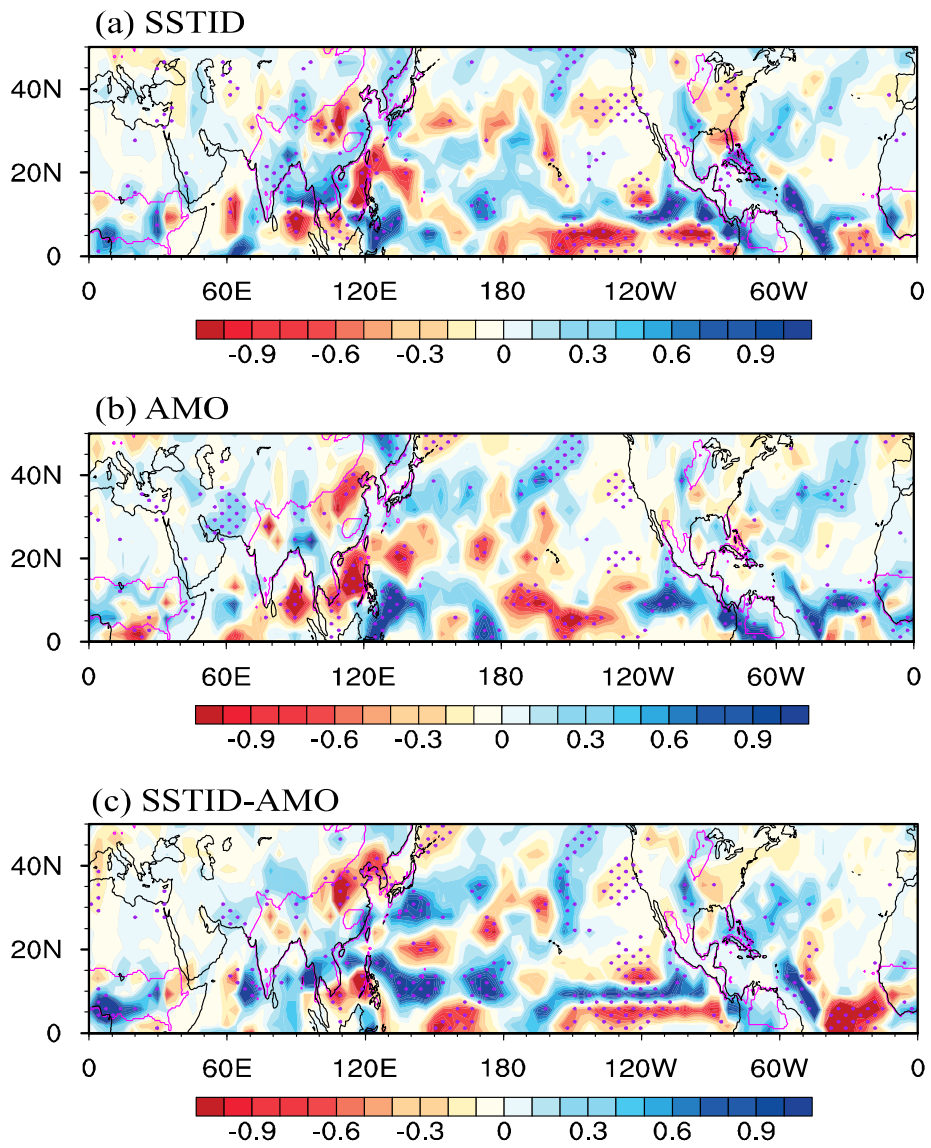

Figure 9. (a) Simulated responses of summer precipitation to the forcing of SSTID anomalies in ICTPAGCM sensitivity experiment. (b), (c) As in (a), but for (b) AMO anomalies and (c) SSTID anomalies removing the AMO signal. The pink lines in the figure outline the land monsoon area in the northern hemisphere. Stippling indicates differences that are significant at the 90% confidence level.

evolutions between the SSTID and ITC, IPC as well as the planetary monsoon circulation in the AMIP experiment are analyzed in figure S6, which demonstrates the SSTID modulates monsoon intensity by changing ITC and pressure gradient. Consequently, results from above AGCM simulations all support the hypothesis that SSTID thermal forcing modulates the decadal variation of NHSM by causing planetary-scale atmospheric circulation adjustments.

4. Summary and discussion

The SSTID, characterized by opposite-signed SST anomalies between the two hemispheres, is one of the dominant modes of global SST variability (Parker *et al* 2007, Sun *et al* 2013, Chen *et al* 2017). In the present study, the SSTID is demonstrated to have significant impacts on the decadal variation of NHSM, with positive phases of the SSTID corresponding to enhanced NHSM. During positive phases of the SSTID, surface air temperature is increased over the northern hemisphere and decreased over the southern hemisphere, thereby enhancing the ITC. Because SLP changes are associated with the air temperature, the increased thermal contrast between the two hemispheres enhances the south–north pressure gradient, which strengthens the northward cross-equatorial airflow and leads to the increase of summer monsoonal circulation and rainfall in the northern hemisphere. Moreover, the SST-forced sensitivity and AMIP simulations are employed to verify the NHSM responses to SSTID thermal forcing.

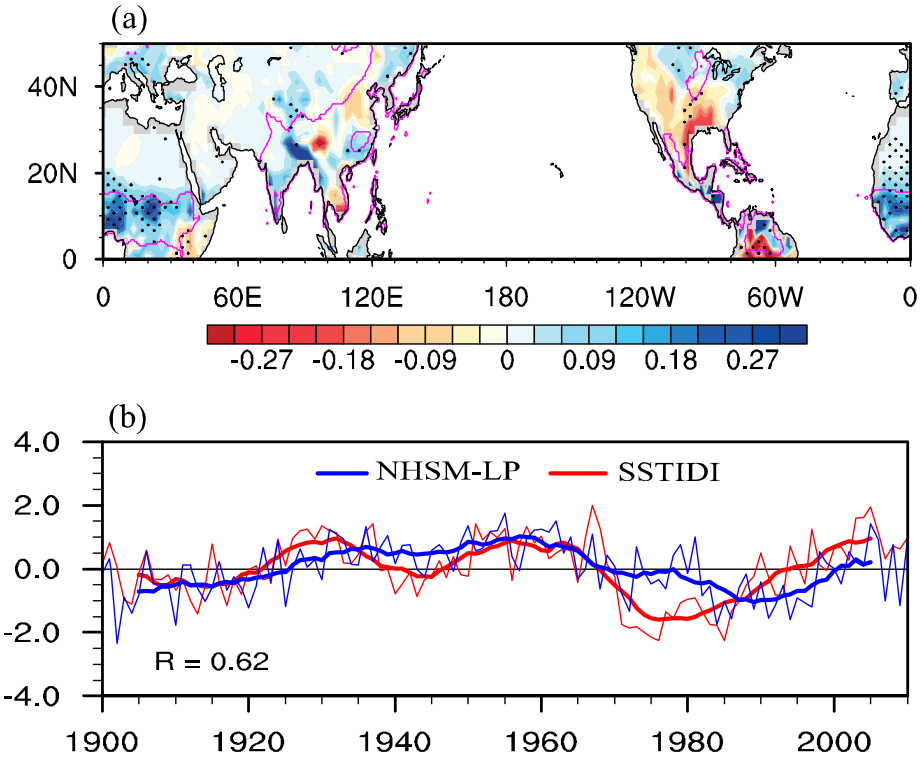

Figure 10. (a) Regression of summer precipitation anomalies onto the normalized SSTID index during 1900–2010 in SST-forced AMIP ensemble simulations. The land monsoon area in the northern hemisphere is outlined by pink lines. Dotted shading indicates regressions significant at the 95% confidence level. (b) Normalized time series of the SSTID index and NHSM-LP index during 1900–2010 and their 11-year running means in AGCM simulations.

Regarding the climate impacts of the SSTID, previous studies found the SSTID can cause equatorial asymmetric responses in tropical rainfall and extratropical atmospheric circulation over the two hemispheres (Sun *et al* 2013, Xue *et al* 2018a). Nevertheless, the potential impacts of the SSTID on global monsoon system remain unknown. In the present study, we demonstrated that SSTID-related thermal forcing also has a significant impact on the decadal variation of NHSM, which further extends our knowledge of the SSTID's climate impacts. This paper primarily focuses on the SSTID's influence on land monsoon variation in the northern hemisphere, where most of the world population lives and long observational data is available. However, oceanic monsoons (e.g. the Western North Pacific monsoon) are also important components of the NHSM (Lee *et al* 2014, Wang and Yu 2018). The decadal variability of NHSM with oceanic monsoons being included deserves further investigation in the future, when observations over the oceans are long enough.

Besides the northern hemisphere monsoon, the southern hemisphere monsoon located in South America, South Africa and Australia is also an essential part of the global monsoon system (Wang and Ding 2006, Zhang 2010, Marengo *et al* 2012, An *et al* 2015). As a global-scale SST mode, the SSTID may also modulate the decadal variability of the southern hemisphere monsoon system, and further exploration of this topic is needed as well.

Data availability statement

The data that support the findings of this study are openly available at the following URL/DOI: https://psl.noaa.gov/data/gridded/.

Acknowledgments

We appreciate the reviewers for helpful comments. This work was jointly sponsored by the National Key Research and Development Program of China (2019YFC1510004), the National Natural Science Foundation of China (42105029, 42130607, 41876020) and The Natural Science Foundation of the Jiangsu Higher Education Institutions of China (21KJB170001). Jiaqing Xue was supported by the Startup Foundation for Introducing Talent of NUIST.

ORCID iD

Jiaqing Xue https://orcid.org/0000-0002-1194-6286

References

An Z *et al* 2015 Global monsoon dynamics and climate change *Annu. Rev. Earth Planet. Sci.* **43** 29–77

Chen X, Wallace J M and Tung K-K 2017 Pairwise-rotated EOFs of global SST *J. Clim.* **30** 5473–89

Chiang J C H and Friedman A R 2012 Extratropical cooling, interhemispheric thermal gradients, and tropical climate change *Annu. Rev. Earth Planet. Sci.* **40** 383–412

Chung E-S and Soden B J 2017 Hemispheric climate shifts driven by anthropogenic aerosol–cloud interactions *Nat. Geosci.* **10** 566–71

Dima M and Lohmann G 2010 Evidence for two distinct modes of large-scale ocean circulation changes over the last century *J. Clim.* **23** 5–16

Dogar M, Kucharski M F and Azharuddin S 2017 Study of the global and regional climatic impacts of ENSO magnitude using SPEEDY AGCM *J. Earth Syst. Sci.* **126** 30

Enfield D B *et al* 2001 The Atlantic multidecadal oscillation and its relation to rainfall and river flows in the continental US *Geophys. Res. Lett.* **28** 2077–80

Folland C K *et al* 1999 Large scale modes of ocean surface temperature since the late nineteenth century *Beyond El Niño: Decadal and Interdecadal Climate Variability* (Berlin: Springer)

Harris I, Jones P, Osborn T and Lister D 2014 Updated high-resolution grids of monthly climatic observations-the CRU TS3.10 dataset *Int. J. Climatol.* **34** 623–42

Henley B J, Gergis J, Karoly D J, Power S, Kennedy J and Folland C K 2015 A tripole index for the interdecadal Pacific oscillation *Clim. Dyn.* **45** 3077–90

Hoerling M, Hurrell J, Eischeid J and Phillips A 2006 Detection and attribution of twentieth-century northern and southern African rainfall change *J. Clim.* **19** 3989–4008

Hsu P-C, Li T and Wang B 2011 Trends in global monsoon area and precipitation over the past 30 years *Geophys. Res. Lett.* **38** 134–44

Huang B, Banzon V F, Freeman E, Lawrimore J, Liu W, Peterson T C, Smith T M, Thorne P W, Woodruff S D and Zhang H-M 2015 Extended reconstructed sea surface temperature version 4 (ERSST.v4). Part I: upgrades and intercomparisons *J. Clim.* **28** 911–30

Kalnay E *et al* 1996 The NCEP/NCAR 40-year reanalysis project *Bull. Am. Meteorol. Soc.* **77** 437–71

Kripalani R H *et al* 2003 Indian monsoon variability in a global warming scenario *Nat. Hazards* **29** 189–206

Kucharski F, Bracco A, Yoo J H, Tompkins A M, Feudale L, Ruti P and Dell'Aquila A 2009 A Gill–Matsuno-type mechanism explains the tropical Atlantic influence on African and Indian monsoon rainfall *Q. J. R. Meteorol. Soc.* **135** 569–79

Kucharski F, Molteni F and Yoo J 2006 SST forcing of decadal Indian Monsoon rainfall variability *Geophys. Res. Lett.* **33** L03709

Lee E-J, Ha K-J and Jhun J-G 2014 Interdecadal changes in interannual variability of the global monsoon precipitation and interrelationships among its subcomponents *Clim. Dyn.* **42** 2585–601

Li H, Dai A, Zhou T and Lu J 2010a Responses of East Asian summer monsoon to historical SST and atmospheric forcing during 1950–2000 *Clim. Dyn.* **34** 501–14

Li J, Wu Z, Jiang Z and He J 2010b Can global warming strengthen the East Asian Summer Monsoon? *J. Clim.* **23** 6696–705

Li J and Zeng Q 2002 A unified monsoon index *Geophys. Res. Lett.* **29** 115-1–115-4

Lopez H, Dong S, Lee S and Goni G 2016 Decadal modulations of interhemispheric global atmospheric circulations and monsoons by the South Atlantic meridional overturning circulation *J. Clim.* **29** 1831–51

Lu R Y, Dong B W and Ding H 2006 Impact of the Atlantic multidecadal oscillation on the Asian summer monsoon *Geophys. Res. Lett.* **33** 194–9

Lyu K, Yu J-Y and Paek H 2017 The influences of the Atlantic multidecadal oscillation on the mean strength of the North Pacific subtropical high during boreal winter *J. Clim.* **30** 411–26

Marengo J A *et al* 2012 Recent developments on the South American monsoon system *Int. J. Climatol.* **32** 1–21

Molteni F 2003 Atmospheric simulations using a GCM with simplified physical parametrizations. I. Model climatology and variability in multi-decadal experiments *Clim. Dyn.* **20** 175–91

Parker D, Folland C, Scaife A, Knight J, Colman A, Baines P and Dong B 2007 Decadal to multidecadal variability and the climate change background *J. Geophys. Res. Atmos.* **112** D18115

Sun C, Kucharski F, Li J, Jin F-F, Kang I S and Ding R 2017 Western tropical Pacific multidecadal variability forced by the Atlantic multidecadal oscillation *Nat. Commun.* **8** 15998

Sun C, Li J, Jin F and Ding R 2013 Sea surface temperature inter-hemispheric dipole and its relation to tropical precipitation *Environ. Res. Lett.* **8** 044006

Taylor K E, Stouffer R J and Meehl G A 2012 An overview of CMIP5 and the experiment design *Bull. Am. Meteorol. Soc.* **93** 485–98

Trenberth K E, Stepaniak D P and Caron J M 2000 The global monsoon as seen through the divergent atmospheric circulation *J. Clim.* **13** 3969–93

Wang B and Ding Q 2006 Changes in global monsoon precipitation over the past 56 years *Geophys. Res. Lett.* **33** 272–88

Wang B, Liu J, Kim H-J, Webster P J, Yim S-Y and Xiang B 2013 Northern hemisphere summer monsoon intensified by mega-El Nino/southern oscillation and Atlantic multidecadal oscillation *Proc. Natl Acad. Sci. USA* **110** 5347–52

Wang L and Yu J-Y 2018 A recent shift in the monsoon centers associated with the tropospheric biennial oscillation *J. Clim.* **31** 325–40

Xue J, Li J, Sun C, Zhao S, Mao J, Dong D, Li Y and Feng J 2018b Decadal-scale teleconnection between South Atlantic SST and southeast Australia surface air temperature in austral summer *Clim. Dyn.* **50** 2687–703

Xue J, Sun C, Li J and Mao J 2018c South Atlantic forced multidecadal teleconnection to the midlatitude south Indian Ocean *Geophys. Res. Lett.* **45** 8480–9

Xue J, Sun C, Li J, Mao J, Nakamura H, Miyasaka T and Xu Y 2018a Divergent responses of extratropical atmospheric circulation to interhemispheric dipolar SST forcing over the two hemispheres in Boreal Winter *J. Clim.* **31** 7599–619

Yun K-S, Ha K-J, Wang B and Ding R 2010 Decadal cooling in the Indian summer monsoon after 1997/1998 El Nino and its impact on the East Asian summer monsoon *Geophys. Res. Lett.* **37** L01805

Zhang H 2010 Diagnosing Australia-Asian monsoon onset/retreat using large-scale wind and moisture indices *Clim. Dyn.* **35** 601–18

Zhang W, Zhou T, Zou L, Zhang L and Chen X 2018 Reduced exposure to extreme precipitation from 0.5 °C less warming in global land monsoon regions *Nat. Commun.* **9** 3153

Zhou T, Gong D, Li J and Li B 2009 Detecting and understanding the multi-decadal variability of the East Asian summer monsoon—recent progress and state of affairs *Meteorol. Z.* **18** 455–67

Zhou T, Yu R, Li H and Wang B 2008 Ocean forcing to changes in global monsoon precipitation over the recent half-century *J. Clim.* **21** 3833–52